GA–A24137

PHYSICS OF ELECTRON CYCLOTRON CURRENT DRIVE ON DIII–D

by

C.C. PETTY, R. PRATER, T.C. LUCE, R.A. ELLIS, R.W. HARVEY,
J.E. KINSEY, L.L. LAO, J. LOHR, and M.A. MAKOWSKI

SEPTEMBER 2002

DISCLAIMER

GA–A24137

PHYSICS OF ELECTRON CYCLOTRON CURRENT DRIVE ON DIII–D

by

C.C. PETTY, R. PRATER, T.C. LUCE, R.A. ELLIS,* R.W. HARVEY,†
J.E. KINSEY,‡ L.L. LAO, J. LOHR, and M.A. MAKOWSKI[Δ]

This is a preprint of a paper to be submitted for publicaton in *Nucl. Fusion.*

*Princeton Plasma Physics Laboratory, Princeton, New Jersey.
†CompX, Del Mar, California.
‡Lehigh University, Bethelehem, Pennsylvania.
[Δ]Lawrence Livermore National Laboratory, Livermore, California.

Work supported by
the U.S. Department of Energy under
Contract Nos. DE-AC03-99ER54463, DE-AC02-76CH03073, W-7405-ENG-48, and Grant Nos. DE-FG03-99ER54541 and DE-FG02-ER54141

GENERAL ATOMICS PROJECT 30033
SEPTEMBER 2002

ABSTRACT

Recent experiments on the DIII-D tokamak have focused on determining the effect of trapped particles on the electron cyclotron current drive (ECCD) efficiency. The measured ECCD efficiency increases as the deposition location is moved towards the inboard midplane or towards smaller minor radius for both co and counter injection. The measured ECCD efficiency also increases with increasing electron density and/or temperature. The experimental ECCD is compared to both the linear theory (Toray-GA) as well as a quasilinear Fokker-Planck model (CQL3D). The experimental ECCD is found to be in better agreement with the more complete Fokker-Planck calculation, especially for cases of high rf power density and/or loop voltage. The narrow width of the measured ECCD profile is consistent with only low levels of radial transport for the current carrying electrons.

1. INTRODUCTION

Electron cyclotron current drive (ECCD) experiments on the DIII-D tokamak are solidifying the physics basis for localized, off-axis current drive, the goal being to validate a predictive model for ECCD [1,2]. Using internal magnetic measurements from motional Stark effect (MSE) polarimetry [3,4], driven currents as small at 1% of the total plasma current can be accurately measured. As a result, the physics of ECCD can be explored in unprecedented detail since the ECCD efficiency can be determined over a wide range of plasma conditions. This is a significant advance over previous ECCD studies on tokamaks and stellarators that mainly measured the magnitude of the driven current from the change in the loop voltage at the plasma surface required to maintain a constant plasma current [5,6].

Electron cyclotron current drive results from the selective heating of electrons traveling in one toroidal direction to decrease their collision frequency, and thus increase their contribution to the toroidal current compared to their unheated counterparts moving in the opposite direction [7,8]. This current drive mechanism is offset by the mirror trapping of electrons in toroidal geometry that drives current in the reverse direction [9]. The opposition between these two current drive mechanisms makes it imperative to study the influence of electron trapping on ECCD, which is done in this paper by determining the current drive dependences as a function of the poloidal deposition location, normalized radius of deposition, and electron beta. The electron trapping effects on the ECCD are measured for both co and counter injection.

The measured ECCD dependences on electron trapping are compared with the theoretical dependences calculated by a bounce-averaged, quasilinear Fokker-Planck model [10], including the effect of the residual parallel electric field ($E_{||}$), which is the most complete model of ECCD available to us. These experiments satisfy all of the underlying theoretical assumptions, such as full absorption of the wave energy before the cold plasma resonance is reached and good confinement of the heated electrons. Radial transport of electrons is normally turned off in the CQL3D modeling since there is no experimental indication of ECCD profile broadening. This paper also compares the experimental ECCD to the theoretical current drive in the $E_{||} = 0$, low power density limit as determined from the linearized Fokker-Planck equation using ray tracing codes [11,12,13,14]. While the linear ECCD efficiency is not expected to accurately predict the experimental results in general, it may be an appropriate approximation in some regimes.

The rest of this paper is organized as follows: in Section 2, the DIII–D tokamak, ECCD system, and current drive analysis methods are described. Section 3 summarizes the dependencies of the ECCD efficiency for various scans that mainly alter the electron trapping effects. A comparison of the experimental ECCD with both linear and quasilinear Fokker-Planck models is shown in Section 4, while the lack of ECCD profile broadening due to radial transport of the energetic electrons is discussed in Section 5. The conclusions are presented in Section 6.

2. EXPERIMENTAL SETUP

These ECCD experiments are done on the DIII-D tokamak [15], typical parameters for which are major radius R = 1.7 m, minor radius a = 0.6 m, elongation κ = 1.8, toroidal magnetic field strength B_T = 1.65–2.15 T, and plasma current I_p = 0.6–1.3 MA. The working gas for plasma fueling and neutral beam injection (NBI) is deuterium. These experiments use up to five gyrotron oscillators operating at 110 GHz, with a maximum combined power of P_{ec} = 2.3 MW injected into the plasma [16,17,18]. The beams from the gyrotrons are launched into the tokamak from the low magnetic field side using a pair of mirrors that allows the poloidal aiming to be changed between plasma pulses. Several gyrotrons are connected to launchers that allow the user to switch between co and counter injection for maximum experimental flexibility. The polarization corresponding to the X-mode dispersion relation is launched in these experiments since it is absorbed strongly near the second harmonic of the electron cyclotron resonance. The polarization, propagation, and deposition of the launched electron cyclotron waves have been confirmed experimentally on DIII-D [19,20,21].

Two separate methods are used on DIII-D to deduce the ECCD from the MSE signals. In the first method, the noninductive current drive is determined from the evolution of the poloidal magnetic flux obtained from a magnetic equilibrium reconstruction constrained by the MSE data [22,23]. The first localized measurements of the ECCD profile were made using this analysis method on DIII-D [24,25]. In the second method, the measured MSE signals are compared to realistic simulations of the MSE evolution using a model of the ECCD profile [1,2]. The parameters of the model — location, width, and magnitude — are adjusted until a best fit between the measured and simulated MSE signals is obtained. Although the two analysis methods have different strengths and weaknesses [1], they give similar results when compared using standard test cases. In this paper, the ECCD results are obtained using the second method exclusively, which has the advantage that arbitrarily narrow current drive profiles can be handled by the direct fits to the raw MSE data.

3. EFFECT OF ELECTRON TRAPPING ON ECCD

The experiments discussed in this section vary the interaction between the electron cyclotron waves and the particles in both velocity space and real space, and primarily test the effect of electron trapping on the ECCD efficiency. Since many of these experiments vary the electron density (n_e) and temperature (T_e), it is convenient to normalize out the usual power per particle and collisionality effects when discussing the current drive efficiency, resulting in a dimensionless ECCD efficiency given by

$$\varsigma_{ec} = \frac{e^3}{\varepsilon_0^2}\frac{I_{ec}Rn_e}{P_{ec}kT_e} = 3.27\frac{I_{ec}(\mathrm{A})R(\mathrm{m})n_{19}}{P_{ec}(\mathrm{W})\,T_e(\mathrm{keV})} \quad , \tag{1}$$

where R is the average major radius of the plasma surface, n_{19} is the electron density in units of 10^{19} m^{-3}, e is the charge of an electron, ε_0 is the permittivity of free space, and k is the Boltzmann constant. The normalization given in Eq. (1) with density and temperature is appropriate for central current drive; however, when electron trapping effects are strong, there are additional n_e and T_e dependences as discussed later in this section. The main tenets of electron trapping theory are examined by determining the ECCD efficiency as a function of the poloidal deposition location (θ_{pol}), normalized radius of deposition (ρ), and electron beta (β_e). Here the poloidal angle is defined to be 0 deg on the outboard midplane, 90 deg at the top of the plasma, and 180 deg on the inboard midplane. Note that the measured ECCD reported in this paper necessarily includes the synergistic current drive that is proportional to both the loop voltage and the ECCD power. Theoretically, the residual loop voltage primarily affects the non-Maxwellian resistivity, resulting in a distorted electron distribution function that leads to a small but measurable modification in the ECCD.

Varying the parallel index of refraction ($N_{||}$) allows the electron trapping effects to be determined for co and counter ECCD separately and tests the velocity space interaction between electron cyclotron waves and electrons. Figure 1 shows that scanning $N_{||}$ from positive to negative values at the point of absorption switches the ECCD from the co to the counter direction, with radial injection ($N_{||} = 0$) driving little current. The value of $N_{||}$ is varied by changing the toroidal injection angle on a shot-to-shot basis. Theoretically, the ECCD efficiency is expected to increase with a larger magnitude of $N_{||}$ since the electron cyclotron waves interact with higher parallel velocity electrons. (However, at too high an $N_{||}$ value there are not enough high energy electrons to damp the waves and this effect diminishes.) In Fig. 1, the measured ζ_{ec} at fixed deposition location (ρ, θ_{pol}) and fixed β_e is seen to increase with larger $|N_{||}|$ for both co and counter injection, in agreement with the theoretical value of ζ_{ec} determined by the CQL3D quasilinear Fokker-Planck code [10], including the effect of $E_{||}$. In this paper, the measured $E_{||}$ profile used in the CQL3D modeling is determined from a loop voltage profile analysis [22].

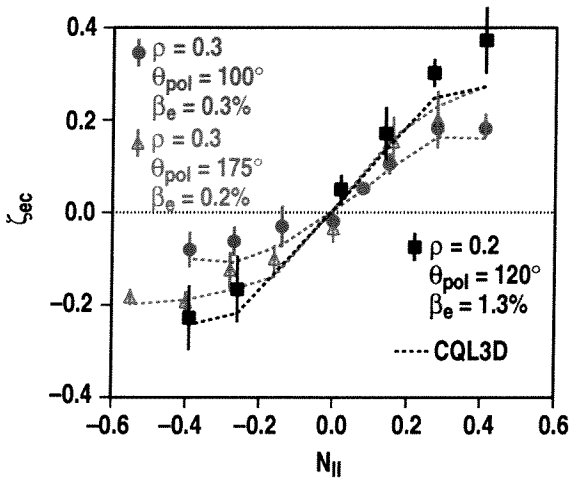

Fig. 1. Experimental dimensionless ECCD efficiency for scans of the parallel index of refraction. The normalized radius and poloidal angle of deposition, and the local electron beta are noted for each scan. The theoretical dependence from the CQL3D code is also shown (dashed lines).

The effect of electron trapping on the dimensionless ECCD efficiency is investigated by varying the poloidal location of the ECCD deposition at constant minor radius. This is effective because the local trapped particle fraction varies from small near the high field side midplane (θ_{pol} = 180°) to maximum at the low field side midplane (θ_{pol} = 0°). Figure 2 shows that the measured ζ_{ec} increases as the poloidal location of deposition is moved towards the high field side at fixed ρ and $N_{||}$. (The maximum B_T of 2.16 T on DIII-D limits the minimum value of θ_{pol} to be ≈60 deg for off-axis deposition.) This effect is especially apparent in low β_e plasmas, while the θ_{pol} dependence for high β_e plasmas is weaker due to the reduced trapping effect at high electron density and temperature, as discussed later in this section. In addition, the θ_{pol} dependence of ζ_{ec} is stronger at larger ρ. The experimental data in Fig. 2 are in agreement with the θ_{pol} dependence predicted by the CQL3D code, including the effect of $E_{||}$, for both co and counter injection. Therefore, it is easiest to drive current off-axis when the ECCD location is on the inboard side of the plasma, but at high β_e the difference between the inboard midplane and the top of the plasma is small.

Another effect of electron trapping is that the ECCD efficiency should decrease with increasing minor radius because the trapped particle fraction increases with increasing ρ. Figure 3 shows that for low beta L-mode plasmas (β_e = 0.4%), the measured ζ_{ec} does decrease rapidly with increasing ρ, in agreement with the theoretical prediction from the CQL3D code. This scan is done at fixed B_T by varying the poloidal steering of the antenna while adjusting the toroidal steering to hold $N_{||}$ fixed. The poloidal deposition location for B_T = 2.0 T is above the plasma axis (θ_{pol} = 95 deg), where the trapped electron fraction is moderately large. This decrease in ζ_{ec} with ρ extrapolates to nearly zero current drive efficiency at ρ ≈ 0.5 in these low beta plasmas. This would be a disappointing outcome for advanced tokamak (AT) scenarios, where the ECCD needs to be located near ρ ≈ 0.5 for current profile control [26,27]. Fortunately, Fig. 3

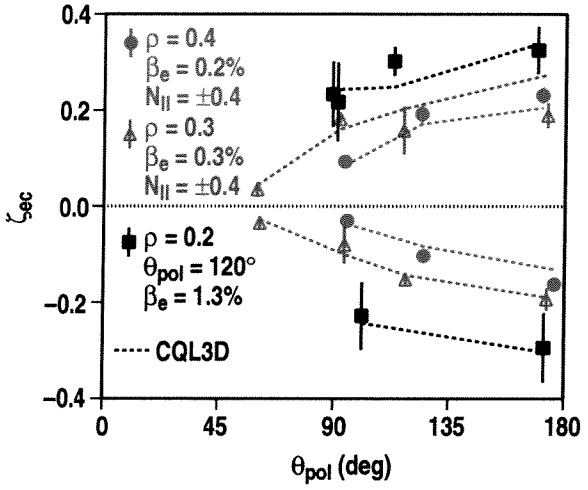

Fig. 2. Experimental dependence of the dimensionless ECCD efficiency on the poloidal angle of deposition, where positive values denote co current drive. The theoretical dependence calculated by the CQL3D code is also shown (dashed lines).

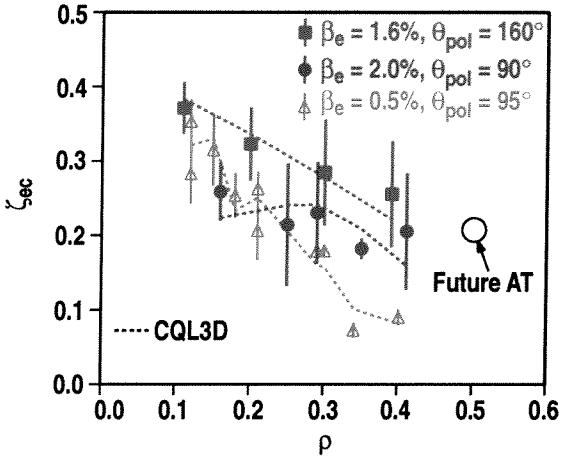

Fig. 3. Experimental dimensionless ECCD efficiency for co injection for scans of the normalized radius of deposition in low beta L-mode and high beta H-mode plasmas. The theoretical dependence calculated by the CQL3D code is also shown (dashed lines).

shows that for high beta H-mode plasmas (β_e = 1.9%) at the same magnetic field strength, the measured ζ_{ec} decreases little with increasing ρ. This is explained theoretically [28] by the shift in the electron cyclotron resonance to higher parallel velocities owing to the stronger damping of electron cyclotron waves at higher electron density and/or temperature as well as relativistic effects. This increases the separation in velocity space between the position of the power deposition on the electron cyclotron resonance curve and the trapped-passing boundary, making the current carrying electrons less likely to pitch angle scatter into the trapped region which increases the current drive efficiency. In addition to the reduced trapping effects, the interaction of electron cyclotron waves with more energetic electrons (owing to the stronger damping) can also lead to an additional increase in the current drive efficiency at higher n_e and T_e. The theoretical ECCD efficiency from the CQL3D code, including the effect of $E_{||}$, is in agreement with the experiment for both the strong trapping and weak trapping situations in Fig. 3. Thus, the theoretical prediction of an ECCD efficiency of $\zeta_{ec} \approx 0.2$ at $\rho = 0.5$ in future AT scenarios [26,27] with $\langle\beta\rangle$ up to 7.5% appears to be achievable experimentally on DIII-D, which should be sufficient to sustain hollow current profiles.

The role that reduced trapping effects play in increasing the ECCD efficiency is confirmed by the radial scan at B_T = 1.8 T in high beta H-mode plasmas (β_e = 1.6%) that is also shown in Fig. 3. The reduced magnetic field strength moves the deposition to the high field side (θ_{pol} = 160 deg) where the trapped particle fraction is lower, resulting in higher measured values of ζ_{ec} that decrease relatively slowly with increasing ρ in agreement with the prediction of the CQL3D code. When the ECCD location is moved to the inboard midplane, the trapped-passing boundary and electron cyclotron resonance curve are shifted as far apart as possible in velocity space; therefore, the favorable beta dependence of ζ_{ec} is expected to become less apparent. This is confirmed experimentally in Fig. 4, where radial scans of the measured ECCD efficiency for

co and counter injection near θ_{pol} = 180 deg are plotted for both H-mode and L-mode plasmas. For these scans, the radius of deposition is varied by changing B_T while the poloidal steering of the antenna is adjusted to keep the deposition near the inboard midplane. In addition, the toroidal steering of the antenna is adjusted to keep $N_{||}$ fixed at ±0.35. The gradual reduction in ζ_{ec} with increasing ρ for both co and counter ECCD indicates that the effects of electron trapping are reduced for deposition on the inboard midplane. In the region around $0.3 < \rho < 0.4$, an increase in the plasma beta from 0.4% to 1.5% hardly changes the measured value of ζ_{ec}. This is in agreement with the CQL3D code, including the effect of $E_{||}$, which predicts that the theoretical ECCD efficiency should change by only ≈10% between these two beta values at this deposition location.

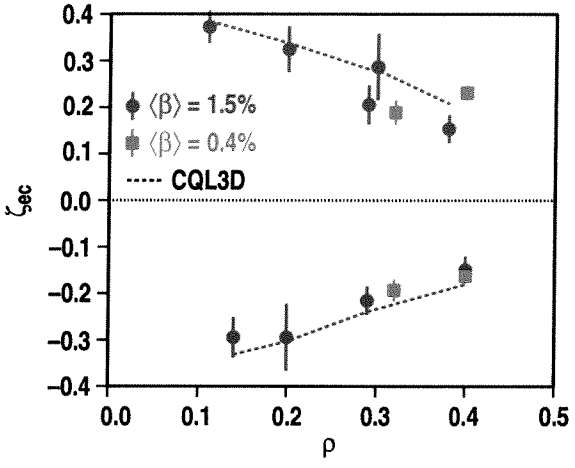

Fig. 4. Measured dimensionless ECCD efficiency for scans of the normalized radius of deposition on the inboard midplane for low beta L-mode and high beta H-mode plasmas. Positive values denote co current drive. The theoretical dependence calculated by the CQL3D code is shown (dashed lines).

4. COMPARISON OF LINEAR AND FOKKER-PLANCK MODELS

The goal of these ECCD experiments is to validate a predictive model of ECCD, with the quasilinear Fokker-Planck code CQL3D [10] representing the most complete model of ECCD that is available to us. The experimental data presented in Section 3 show that the measured ECCD on DIII-D is in good agreement with the CQL3D code, including the effect of $E_{||}$, for both co and counter injection over a wide range of conditions. However, since it is also a common practice to calculate the theoretical ECCD from the relativistic, linearized Fokker-Planck equation using ray tracing codes [11,12,13,14], it is worthwhile to make a detailed comparison between the experimental data and both the linear model and quasilinear Fokker-Planck model. It is especially important to determine if the physics improvements in the more complete Fokker-Planck model (*i.e.*, d.c. parallel electric field, rf quasilinear diffusion, momentum conservation in electron-electron collisions) actually bring theory and experiment into better agreement or not.

First, if the effect of the parallel electric field is neglected in the CQL3D calculation, then the agreement between theory and experiment declines for co injection. Figure 5 shows the ratio of the measured and theoretical co ECCD as a function of the measured $E_{||}$ normalized to the critical field (E_{cr}) [29] for runaway of thermal electrons at the ECCD location. In Fig. 5, $E_{||}$ at the ECCD deposition location is determined from the evolution of the poloidal magnetic flux given by equilibrium reconstructions constrained by the MSE data [22]. A statistical comparison between the CQL3D model with $E_{||} = 0$ and the measured ECCD for the dataset in Fig. 5 yields a reduced χ^2 of 1.8, which is significantly larger than the reduced χ^2 of 1.0 for the comparison where $E_{||}$ is retained in the CQL3D modeling. There is some uncertainty in the injected ECCD power that is not included in the error bars in Fig. 5, but the statistical comparison over a large number of points reduces the effect of this problem. Figure 5 also shows that the inclusion of the parallel electric field in the theory most affects the cases that have large values of $E_{||}/E_{cr}$, as expected.

Second, if the linear ECCD efficiency calculated by the Toray-GA code is used, then the agreement between theory and experiment becomes worse for co injection. Figure 6 shows the ratio of the measured and theoretical co ECCD as a function of the rf power density (Q_{ec}) normalized to the square of the electron density at the ECCD location. The main differences between the two theoretical models in Fig. 6 are the neglect in Toray-GA of nonthermal effects as well as the neglect in Toray-GA of momentum conservation in electron-electron collisions. A statistical comparison between Toray-GA and the measured ECCD for the dataset in Fig. 6 gives a reduced χ^2 of 6.4, which is larger than the reduced χ^2 of 1.8 for the CQL3D model with $E_{||}$ set to zero (to be consistent with the neglect of $E_{||}$ in the linear theory). Theoretically, the ECCD efficiency is expected to be power dependent at high rf power densities [30], *i.e.*, Q_{ec} (MW/m^3) $\geq 0.5\ [n_e\ (10^{19}\ \text{m}^{-3})]^2$. Figure 6 clearly shows that the largest discrepancies between the Toray-

GA code and experiment occur for rf power densities above this level. However, the linear theory also slightly under predicts the measured co ECCD by ≈15% (relative to CQL3D) even for low values of Q_{rf}. This is mostly explained by the neglect of momentum conservation in electron-electron collisions in Toray-GA, which is calculated to be a 10% effect by CQL3D, although this is not the only difference between these two codes in this limit. While the linear theory is a relatively good predictor of co ECCD for low rf power densities (and presumably low loop voltages), it is also interesting to note that for counter injection both Toray-GA and CQL3D agree with the measured ECCD equally well. This appears to be a fortuitous result for the linear theory because the neglect of nonthermal effects and momentum conservation in Toray-GA, which underestimates the ECCD magnitude, tends to offset the neglect of $E_{||}$, which overestimates the ECCD magnitude for counter injection. Nevertheless, taking the whole ECCD dataset on DIII–D into account, the more complete quasilinear Fokker-Planck theory of ECCD, including the effect of $E_{||}$, is clearly the better predictor of the experimental ECCD efficiency.

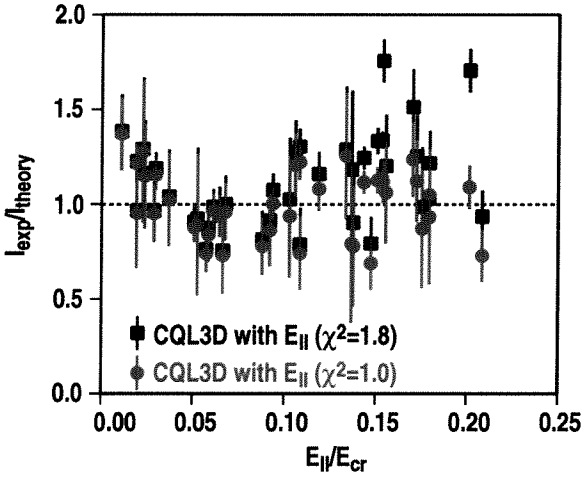

Fig. 5. Ratio of measured and theoretical ECCD as a function of the d.c. parallel electric field normalized to the critical field. The theoretical ECCD is calculated by the CQL3D code with and without including the effect of $E_{||}$.

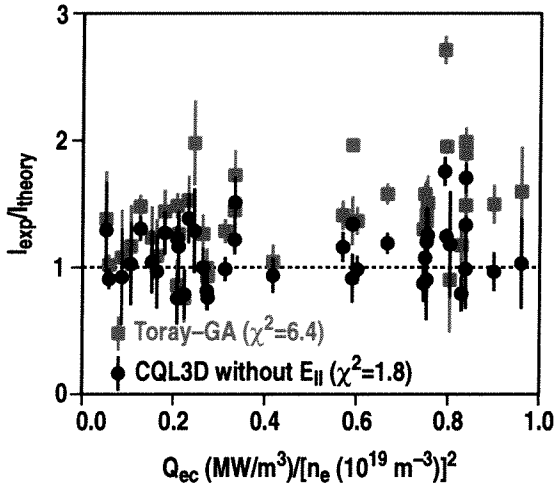

Fig. 6. Ratio of measured and theoretical ECCD as a function of the relative rf power density. The theoretical ECCD is calculated by the linear Toray-GA code and the quasilinear CQL3D code (not including the effect of $E_{||}$).

5. EFFECT OF RADIAL TRANSPORT ON PROFILE WIDTH

So far in this paper, the effect of radial transport of the current carrying electrons on the radial profile of ECCD has been neglected. Although the comprehensive CQL3D code is capable of modeling the effects of radial transport on the ECCD profile, this capability has not yet been utilized in this paper because there is no experimental indication on DIII-D of ECCD profile broadening caused by radial transport of energetic electrons. The narrow ECCD profile obtained from the evolution of the poloidal magnetic flux is found to agree with the CQL3D code with radial transport turned off when a local representation is used in the MSE-constrained equilibrium reconstructions [23]. Furthermore, ECCD experiments on DIII-D have demonstrated that all of the driven current can be situated across a single MSE channel with a spatial resolution of just 0.05 m, in good agreement with the theoretical profile width in the absence of radial transport (Fig. 8 of Ref. [1] and Fig. 2 of Ref. [2]). However, recently it has been shown that the transport effect on ECCD in the TCV tokamak is overwhelming [31], where the inclusion of radial transport in the CQL3D code at levels given by the global energy confinement decreases the predicted ECCD magnitude by more than a factor of five and substantially broadens the ECCD profile, bringing the CQL3D code predictions in line with experimental measurements on TCV. Similar modeling in Ref. [31] for DIII-D predicts that the redistribution of current-carrying electrons due to similar levels of radial transport should broaden the ECCD profile by nearly a factor of three, although the ECCD magnitude should be reduced by less than 10% since the energetic electrons are well confined on DIII-D. Spreading of the driven current by this amount would have a detrimental effect on the ability of ECCD to stabilize neoclassical tearing modes [32].

In this section, MSE measurements of the ECCD profile width on DIII-D are compared with CQL3D modeling to place an upper bound on the level of radial transport of the current-carrying electrons. The DIII-D discharge (#104017) modeled in Fig. 5 of Ref. [31] will be used for this purpose. This discharge is a low current (I_p = 0.6 MA) L-mode plasma with 2.4 MW of NBI and 1.1 MW of ECCD located at $\rho = 0.3$. The measured change in the toroidal current density profile (ΔJ_ϕ) between this co ECCD discharge and a similar discharge without ECCD is shown in Fig. 7, where J_ϕ is determined directly from the MSE measurement of the vertical component of the magnetic field (B_z) as a function of major radius (R) using the relation [33]

$$\mu_0 \; J_\phi = -\frac{B_z}{\kappa^2 \left(R - R_0\right)} - \frac{\partial B_z}{\partial R} \quad . \tag{2}$$

Here R_0 is the major radius of the plasma axis, with R_0 = 1.76 m for this discharge. Figure 7 shows that co ECCD causes the measured J_ϕ to increase in a very localized region around the

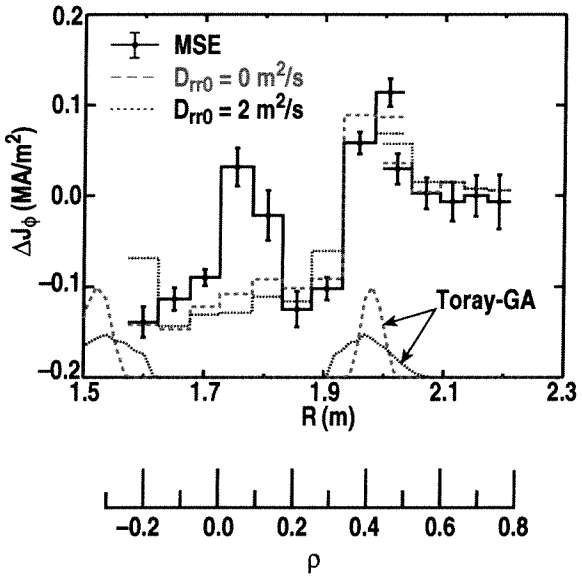

Fig. 7. Change in the measured (solid lines) and simulated (dashed lines) toroidal current density as a function of major radius between discharges with and without co ECCD. The magnetic axis is at R_0 = 1.76 m, and the ECCD profiles from Toray-GA used in the simulations to reproduce the broadening effects of radial transport are also indicated (not to scale).

expected current drive location on the outboard midplane. Inside of this location, the measured J_ϕ decreases owing to a reduction in the ohmic current since the total plasma current is held fixed. Also in Fig. 7, the MSE measurements are compared to simulations of the MSE signals using the ONETWO transport code [1,26] for two different ECCD profile widths that correspond to CQL3D calculations with and without radial transport. The CQL3D modeling used in this section includes a radial diffusion coefficient that increases towards the periphery, $D_{rr} = D_{rr0}\ (1 + 3\ \rho^3)\ [n_{e0}/n_e(\rho)]$, and a pinch term that is adjusted to maintain a target experimental density profile [31]. Since the ONETWO code is not coupled to CQL3D, the Toray-GA ray tracing code is used instead to simulate the ECCD profiles calculated by CQL3D. The profile widths determined by Toray-GA and CQL3D are essentially the same for the case without radial transport ($D_{rr0} = 0$), whereas the profile width determined by CQL3D for levels of radial transport consistent with global energy confinement ($D_{rr0} = 2\ m^2s^{-1}$) is reproduced in Toray-GA by artificially spreading the beam width. Figure 7 shows that the simulation with $D_{rr0} = 0$ better matches the measured MSE data near the ECCD locations than does the simulation with $D_{rr0} = 2\ m^2s^{-1}$.

A statistical comparison between the measured and simulated MSE signals for a variety of ECCD profile widths shows that the best agreement is obtained for the narrow profile expected in the absence of significant radial transport. The ECCD profile width is scanned in the ONETWO simulations by varying the spreading of the beam width in Toray-GA while keeping fixed the integrated current drive and the resonance location. The spreading of the beam width is gauged to reproduce the change in the ECCD profile as calculated by CQL3D for diffusion

coefficients between $D_{rr0} = 0$ and $D_{rr0} = 4\ m^2s^{-1}$. Figure 8(a) shows the χ^2 from a statistical comparison between the measured and simulated ΔJ_ϕ calculated using Eq. (2) as a function of the normalized width of the driven current; the corresponding values of D_{rr0} needed to achieve those widths in CQL3D are displayed in Fig. 8(b). Figure 8 shows that the simulated MSE data agrees best with measurement for the most narrow ECCD profile width that is possible, and that values of D_{rr0} greater than $0.25\ m^2s^{-1}$ give profile widths that are wider than the experiment supports. This upper bound to D_{rr0} is significantly less than the level of radial transport from global energy confinement ($D_{rr0} = 2\ m^2s^{-1}$), but it is comparable to the effective (including pinch) particle diffusion coefficient at $\rho = 0.3$ for this discharge ($D_{eff} = 0.2\ m^2s^{-1}$).

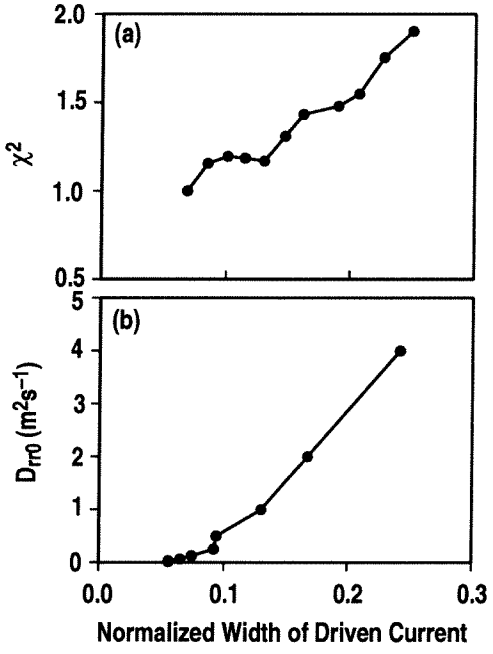

Fig. 8. (a) Goodness of fit between the measured and simulated profiles of ΔJ_ϕ as a function of the normalized ECCD profile width, and (b) the diffusion coefficients needed to achieve those widths in CQL3D.

6. CONCLUSIONS

Recent experiments on the DIII-D tokamak have made great progress in validating a predictive model of ECCD, especially in regard to the effects of electron trapping. The measured ECCD switches from the co to the counter direction as the toroidal injection angle is varied, with radial injection driving little current. The current drive efficiency for both co and counter ECCD is measured to increase as the poloidal location of deposition is moved from the low field side to the high field side of the machine, which is expected since the local trapped electron fraction is lower near the inboard midplane. In low beta plasmas, the experimental ECCD efficiency decreases rapidly as the deposition is moved off-axis towards the top of the machine, but this radial dependence becomes much weaker in high beta plasmas. Thus, the detrimental effects of electron trapping on the ECCD efficiency are greatly diminished at high electron density and/or temperature. Owing to this favorable density/temperature dependence, high ECCD efficiencies for off-axis deposition are expected in future high beta advanced tokamak plasmas. The measured ECCD is in good agreement with the CQL3D quasilinear Fokker-Planck code, including the effect of the residual parallel electric field, over a wide range of conditions. The narrow width of the measured ECCD profile matches the CQL3D calculation in the absence of radial transport; thus, radial transport of current-carrying electrons must be at low levels on DIII-D. Although the differences in the theoretical ECCD calculated by the CQL3D code and linear theory are small at low rf power densities and low parallel electric fields, the experimental data clearly show that the more complete quasilinear Fokker-Planck modeling is required to obtain good agreement with measurements at high rf power densities and/or high parallel electric fields.

REFERENCES

[1] C.C. Petty, *et al.,* Nucl. Fusion **41**, 551 (2001).

[2] C.C. Petty, *et al.,* "Detailed Measurements of the Electron Cyclotron Current Drive Efficiency on DIII-D," to be published in Nucl. Fusion.

[3] F.M. Levinton, *et al.,* Phys. Rev. Lett. **63**, 2060 (1989).

[4] B.W. Rice, K.H. Burrell, L.L. Lao, Y.R. Lin-Liu, Phys. Rev. Lett. **79**, 2694 (1997).

[5] V. Erckmann, V. Gasparino, Plasma Phys. Control. Fusion **36**, 1869 (1994).

[6] B. Lloyd, Plasma Phys. Control. Fusion **40**, A119 (1998).

[7] N.J. Fisch, A.H. Boozer, Phys. Rev. Lett. **45**, 720 (1980).

[8] N.J. Fisch, Rev. Mod. Phys. **59**, 175 (1987).

[9] T. Ohkawa, "Steady-State Operation of Tokamaks by rf Heating," General Atomics Report GA-A13847 (1976).

[10] R.W. Harvey, M.G. McCoy, in Proc. of the IAEA Technical Committee Meeting, Montreal, 1992 (IAEA, Vienna, 1993) 498.

[11] A.H. Kritz, H. Hsuan, R.C. Goldfinger, D.B. Batchelor, in Proc. of the 3rd Int. Symposium on Heating in Toroidal Plasmas, Grenoble, 1982, Vol. II (Brussels, CEC) p. 707.

[12] R.H. Cohen, Phys. Fluids **30**, 2442 (1987).

[13] K. Matsuda, IEEE Trans. Plasma Sci. **17**, 6 (1989).

[14] Y.R. Lin-Liu, *et al.*, Controlled Fusion and Plasma Physics (Proc. 26th Euro. Conf., Maastricht, 1999), Vol. 23J (European Physical Society, Geneva, 1999) p 1245.

[15] J.L. Luxon, Nucl. Fusion **42**, 614 (2002).

[16] R.W. Callis, *et al.*, Fusion Technol. (Proc. 20th Symp. Marseille, 1998), Vol. 1, Association EURATOM-CEA, Saint-Paul-Lez-Durance (1998) 315.

[17] J. Lohr, *et al.*, Infrared and Millimeter Waves (Proc. 23rd Int. Conf., Colchester, 1998), University of Essex, Colchester (1998) 269.

[18] J. Lohr, *et al.*, Radiofrequency Power in Plasmas (Proc. 14th Int. Conf., Oxnard, 2001), AIP, New York (2001) 314.

[19] C.C. Petty, *et al.*, Radiofrequency Power in Plasmas (Proc. 13th Int. Conf., Annapolis, 1999), AIP, New York (1999) 245.

[20] C.C. Petty, *et al.*, Strong Microwaves in Plasmas (Proc. 4th Int. Conf., Nizhny Novgorod, 1999), Vol. 1, Russian Academy of Sciences, Nizhny Novgorod (2000) 41.

[21] C.C. Petty, *et al.*, Radiofrequency Power in Plasmas (Proc. 14th Int. Conf., Oxnard, 2001), AIP, New York (2001) 275.

[22] C.B. Forest, *et al.*, Phys. Rev. Lett. **73**, 2444 (1994).

[23] L.L. Lao, *et al.*, Radiofrequency Power in Plasmas (Proc. 14th Int. Conf. Oxnard, 2001), AIP, New York (2001) 310.

[24] T.C. Luce, *et al.*, Phys. Rev. Lett. **83**, 4550 (1999).
[25] T.C. Luce, *et al.*, Plasma Phys. and Control. Fusion **41** B119 (1999).
[26] H.E. St. John, T.S. Taylor, Y.R. Lin-Liu, A.D. Turnbull, Plasma Physics and Controlled Nuclear Fusion Research 1994 (Proc. 15th Int. Conf., Seville, 1994), Vol. 3 (IAEA, Vienna, 1996) p. 603.
[27] A.D. Turnbull, T.S. Taylor, Y.R. Lin-Liu, H.E. St. John, Phys. Rev. Lett. **74**, 718 (1995).
[28] R. Prater, R.W. Harvey, Y.R. Lin-Liu, T.C. Luce, C.C. Petty, Radiofrequency Power in Plasmas (Proc. 14th Int. Conf., Oxnard, 2001), AIP, New York (2001) 302.
[29] H. Knoepfel, D.A. Spong, Nucl. Fusion **19**, 785 (1979).
[30] R.W. Harvey, M.G. McCoy, G.D. Kerbel, Phys. Rev. Lett. **62**, 426 (1989).
[31] R.W. Harvey, O. Sauter, R. Prater, P. Nikkola, Phys. Rev. Lett. **88**, 205001 (2002).
[32] F.W. Perkins, R.W. Harvey, M. Makowski, M.N. Rosenbluth, Controlled Fusion and Plasma Physics (Proc. 24th Euro. Conf., Berchtesgaden, 1997), Vol. 21A (European Physical Society, Geneva, 1997) p 1017.
[33] C.C. Petty, W.R. Fox, T.C. Luce, M.A. Makowski, T. Suzuki, Nucl. Fusion **42**, 1124 (2002).

ACKNOWLEDGMENT

Work supported by the U.S. Department of Energy under Contracts DE-AC03-99ER54463, DE-AC02-76CH03073, and W-7405-ENG-48, and Grants DE-FG03-99ER54541 and DE-DE-FG02-92ER54141.